mater.scichina.com link.springer.com

Published online 23 January 2024 | https://doi.org/10.1007/s40843-023-2741-4
Sci China Mater 2024, 67(3): 898–905

Full β-Ga_2O_3 films-based p-n homojunction

Hongchao Zhai[1], Chenxing Liu[1], Zhengyuan Wu[1,2], Congcong Ma[1], Pengfei Tian[1], Jing Wan[1], Junyong Kang[3], Junhao Chu[2] and Zhilai Fang[1,2*]

ABSTRACT Fabricating the p-n junction and exploring the device physics play key roles in developing various functional devices and promoting their practical applications. Although ultrawide bandgap semiconductors have great potentials to fabricate high-voltage and high-efficiency power devices, the lack of p-type Ga_2O_3 poses a fundamental obstacle for fabricating the Ga_2O_3 p-n homojunction and impedes the development of full Ga_2O_3-based bipolar devices. In this study, n-type Sn-doped β-Ga_2O_3/p-type N-doped β-Ga_2O_3 films are prepared by a novel phase-transition growth technique combined with sputter deposition. Full β-Ga_2O_3 one-sided abrupt p-n homojunction diodes are fabricated and the device physics are explored in detail. The diodes possess a high rectification ratio of 4 × 10^4, a low specific on-resistance of 9.18 mΩ cm^2 at 40 V, a built-in potential of 4.41 V, and an ideal factor of 1.78, and also show a good rectification behavior under alternating voltage with no overshoot and longterm stability. Our results clear away the major obstacle to β-Ga_2O_3 p-n homojunction, lay the foundation for β-Ga_2O_3 homogeneous bipolar devices, and pave the way for the evolution of high-voltage and high-power device applications.

Keywords: gallium oxide, p-n junction, forward characteristics, rectification ratio, specific on-resistance

INTRODUCTION

The p-n junction plays a critical role as the basic device structure for fabricating various electronic and optoelectronic devices. Fabricating the p-n junction and exploring the device physics are crucial to develop functional devices and advance their practical applications. Ultrawide bandgap semiconductors have great potentials to fabricate high-voltage and high-efficiency power devices, which are expected to overcome the limited power capability of Si-based electronic devices. However, the asymmetric doping effect in ultrawide bandgap semiconductors makes it very difficult to achieve efficient bipolar doping, thereby impeding the development of p-n homojunction and the related bipolar devices [1–3]. Monolithic gallium oxide (β-Ga_2O_3) possesses an ultrawide bandgap (E_g, ~4.85 eV) and high Baliga's figure of merit (3444), and promises high-performance power device applications. While n-type β-Ga_2O_3 has been achieved by Sn, Si or Ge doping with good modulation of electron concentration [4], p-type Ga_2O_3 with good conductivity and stability is still difficult to realize due to its large acceptor ionization energy, low hole activation efficiency, hole-trapping effect, self-compensation effect, and low hole mobility [5–8]. The lack of p-type Ga_2O_3 poses a fundamental obstacle for fabricating Ga_2O_3 p-n homojunction and impedes the development of full Ga_2O_3-based materials and devices.

Great efforts have been made to fabricate the Ga_2O_3-based p-n heterojunction *via* combining p-type NiO, CuO, GaN, SiC, or Si with n-type Ga_2O_3 [9–15]. The fabrication of ideal Ga_2O_3-based p-n heterojunction diodes with superhigh electronic and optoelectronic performance still faces some issues, such as piezoelectric effects from lattice mismatch and thermal mismatch [16,17], band offsets, electron traps from bandgap mismatch and heterointerface-induced defects [18], differences in critical electric field (E_c), thermal conductivity, and dielectric constant [19]. Various complex fabrication technologies have to be developed to overcome these issues. In comparison, the p-n homojunction is of mature and diverse fabrication technologies, which makes it simple to design junction structures for functional electronic and optoelectronic devices. Fabrication of p-type Ga_2O_3 and p-n homojunction is of urgency, general scientific significance, technological application significance and enormous economic benefits.

Recently, intrinsic weak p-type β-Ga_2O_3 films with a room-temperature hole concentration of ~2 × 10^{14} cm^{-3} and a Hall resistivity of 10^4 Ω cm are fabricated by annealing β-Ga_2O_3 in oxygen atmosphere [20]. By introducing metal acceptor dopants (Mg, Cu, Se, Zn, etc.), the fabricated β-Ga_2O_3 films are semi-insulting [21–29], which cannot meet the requirements for fabricating high-performance Ga_2O_3 p-n homojunction devices. N-doped β-Ga_2O_3 films with good p-type conductivity and stability are demonstrated recently [30,31]. In this study, β-Ga_2O_3 films with an n-type Sn-doped β-Ga_2O_3/p-type N-doped β-Ga_2O_3 structure are prepared by the growth of ~1.2-μm thick N-doped β-Ga_2O_3 thin film *via* a phase-transition technique, followed by sputter deposition of ~1-μm thick Sn-doped β-Ga_2O_3 thin film. The as-fabricated one-sided abrupt β-Ga_2O_3 thin film p-n homojunction diodes possess a high rectification ratio of 4 × 10^4, a low specific on-resistance ($R_{on,sp}$) of 9.18 mΩ cm^2 at 40 V, an extremely high forward current density of 4.32 × 10^3 A cm^{-2} at 40 V, a built-in potential (V_{bi}) of 4.41 V, a junction depletion width of 0.8 μm, and an ideal factor of 1.78,

[1] Academy for Engineering and Technology, and School of Information Science and Technology, Fudan University, Shanghai 200433, China
[2] Institute of Optoelectronics, Fudan University, Shanghai 200433, China
[3] Collaborative Innovation Center for Optoelectronic Semiconductors and Efficient Devices, Department of Physics, Xiamen University, Xiamen 361005, China
[*] Corresponding author (email: zlfang@fudan.edu.cn)

and also show a good rectification behavior under alternating current (AC) voltage with no overshoot and longterm stability. Our results clear away the major obstacle to β-Ga_2O_3 p-n homojunction, lay the foundation for β-Ga_2O_3 homogeneous bipolar devices, and pave the way for the evolution of high-voltage and high-power device applications.

EXPERIMENTAL SECTION

Materials growth and device fabrication

N-doped β-Ga_2O_3 films were prepared by thermal oxidation of the undoped GaN films at 1150°C, during which a multi-step phase transition from (0001) GaN to ($\bar{2}01$) β-Ga_2O_3 and an *in-situ* N doping in β-Ga_2O_3 were achieved. At the intermediate growth stage of β-Ga_2O_3 films, the GaN films were partially oxidized with distinct β-Ga_2O_3/GaN interfaces. Sample SP with the β-Ga_2O_3/GaN interfaces was prepared for growth evolution analysis. The growth rate, crystalline quality, and N doping of β-Ga_2O_3 films were controlled by oxygen pressure and Ar gas purge. More details for the growth of N-doped β-Ga_2O_3 films could be found in literature [30].

To fabricate the Ga_2O_3 homojunction diode, a pattern was first made on N-doped β-Ga_2O_3 films by ultraviolet lithography (SUSS MA6) followed by development. Then, Sn-doped Ga_2O_3 films were deposited on the N-doped β-Ga_2O_3 films by radio-frequency magnetron sputtering (RFMS, DETECH DE500) using a Sn-doped Ga_2O_3 ceramic target wafer (Sn:Ga = 1:99 wt%, purity 99.99%, ZhongNuo Advanced Material Technology Co., Ltd.). The as-deposited Sn-doped Ga_2O_3/N-doped β-Ga_2O_3 films were annealed in an oxygen atmosphere at 900°C for 120 min for the β phase crystallization of Sn-doped Ga_2O_3 layer. Then, the electrode patterns were both made on the Sn-doped β-Ga_2O_3 layers and the N-doped β-Ga_2O_3 layers of Sn-doped β-Ga_2O_3/N-doped β-Ga_2O_3 films by ultraviolet lithography. Ti (50 nm)/Au (100 nm) electrodes were deposited on the as-photoetched Sn-doped β-Ga_2O_3/N-doped β-Ga_2O_3 films by electron beam evaporation (EBE, DETECH DE400). After a lift-off process, Sn-doped β-Ga_2O_3/N-doped β-Ga_2O_3 homojunction diodes were achieved.

N-doped β-Ga_2O_3 top-gate field effect transistor (FET) was fabricated by depositing 200-nm HfO_2 gate insulator layer and Ti (50 nm)/Au (100 nm) electrodes on N-doped β-Ga_2O_3 films by ultraviolet lithography, atomic layer deposition (Picosun R-200) and EBE. Sn-doped β-Ga_2O_3 back-gate FET was fabricated by depositing ~500-nm Sn-doped β-Ga_2O_3 and Ti (50 nm)/Au (100 nm) electrodes on the silicon-on-insulator substrate by RFMS and EBE.

Materials characterization and device measurement

Microstructures of the Ga_2O_3/GaN interface were studied by high-resolution transmission electron microscopy (HRTEM) combined with the selected area electron diffraction (SAED). Surface chemical information of β-Ga_2O_3 was studied by X-ray photoelectron spectroscopy (XPS). Valence band (VB) photoemission was studied by ultraviolet photoelectron spectroscopy (UPS) and XPS. Spatial and depth distributions of Ga, O, N, Sn, and Al elements were analyzed by secondary-ion mass spectrometry (SIMS). The crystalline structure was investigated by X-ray diffraction (XRD). The vibration modes of β-Ga_2O_3 were studied by Raman spectroscopy. Carrier type, carrier concentration and carrier mobility of N-doped and Sn-doped β-Ga_2O_3 were investigated by van der Pauw Hall effect measurements. Current–voltage (*I*–*V*) characteristics, capacitance–voltage (*C*–*V*) characteristics, and time-dependent electric characteristics were characterized using a semiconductor parameter analyzer (PRIMARIUS FS-Pro).

Simulation method

A stable 120-atom supercell of N-doped β-Ga_2O_3 was constructed and investigated using density functional theory (DFT) calculations, as implemented in the Vienna *Ab Initio* Simulation Package, within the generalized gradient approximation by Perdew–Burke–Ernzerhof. The supercell of N-doped β-Ga_2O_3 with nitrogen impurities at O(III) substitutional site is defined as β-Ga_2O_3:$N_{O(III)}$ (Fig. S1). A screened hybrid functional of Heyd–Scuseria–Ernzerhof (HSE) is employed to examine the formation energies and thermodynamic transition levels of β-Ga_2O_3:N_O. In the HSE(α,μ) function, the Fock-exchange mixing parameter α and the screening parameter μ are set as 0.35 and 0.18 $Å^{-1}$, respectively. The formation energies of β-Ga_2O_3:N_O formed through phase transition from GaN can be given by $E^f(N_O^q) = E_{tot}(N_O^q) - E_{tot}(GaN_xO_{3(1-x)/2}) + n\mu_N - n\mu_O + q(E_{VBM} + E_F + E_{corr})$ ($0 \leqslant x \leqslant 1$), where $E_{tot}(N_O^q)$ denotes the total energy of the supercell for β-Ga_2O_3 crystal containing an N impurity in charge state q, $E_{tot}(GaN_xO_{3(1-x)/2})$ is the total energy of a supercell for the $GaN_xO_{3(1-x)/2}$ crystal, μ_N is the chemical potential of N atoms in the GaN unit cell, μ_O is the chemical potential of O atoms, E_{VBM} is the energy level of VB maximum (VBM), E_F is the Fermi level referenced to E_{VBM}, and E_{corr} is an electrostatic correction associated with spurious electrostatic interactions in a finite-sized charged supercell. The thermo-dynamic transition levels $\varepsilon(0/-)$ of phase from $Ga_{48}O_{70}N_2$ to β-Ga_2O_3:N_O^- are given by $E^f[N_O^-(Ga_{48}O_{71}N_1), E_F = 0] - E^f[N_O^0(Ga_{48}O_{70}N_2), E_F = 0]$, where $E^f[N_O^-(Ga_{48}O_{71}N_1), E_F = 0]$ and $E^f[N_O^0(Ga_{48}O_{70}N_2), E_F = 0]$ denote the formation energies of N_O with the negative and zero charge states, respectively.

Silvaco technology computer-aided design (TCAD) was used to simulate the β-Ga_2O_3 p-n junction. A structure composed of a 1.0-μm thick p-type β-Ga_2O_3 layer (hole concentration: 1.50×10^{15} cm^{-3}), a 1.2-μm thick p-type β-Ga_2O_3 layer (electron concentration: 1.69×10^{16} cm^{-3}), two Ohmic contact electrodes and the sapphire substrate was modeled (Fig. S2a). The *I*–*V* characteristics and band diagram were obtained.

RESULTS AND DISCUSSION

n-type Sn-doped β-Ga_2O_3/p-type N-doped β-Ga_2O_3 films

HRTEM images of Sample SP obtained at different locations of the β-Ga_2O_3/GaN interface show multi-step structural phase transitions ($P6_3mc \rightarrow P6_3mc$-like$\rightarrow R\bar{3}c \rightarrow C2/m$-like$\rightarrow C2/m$) from GaN layer to α-$GaN_xO_{3(1-x)/2}$ layer and eventually to monolithic N-doped β-Ga_2O_3 layer (Fig. 1a). The curve of formation energy *versus* the chemical potential of O atoms $\Delta\mu_O$ (Fig. 1b) with $\Delta\mu_O$ between 0 eV (O-rich) and −3.69 eV (Ga-rich) indicates a good solubility of N dopant in β-Ga_2O_3:$N_{O(III)}$. The (0/−) transition level of the $N_{O(III)}$ acceptor is as low as 0.36 eV (Fig. 1c), indicating the feasibility to achieve p-type N-doped β-Ga_2O_3 films *via* the phase-transition technique. In the following discussion, completely converted N-doped β-Ga_2O_3 films without a GaN bottom layer were employed for materials characterization and

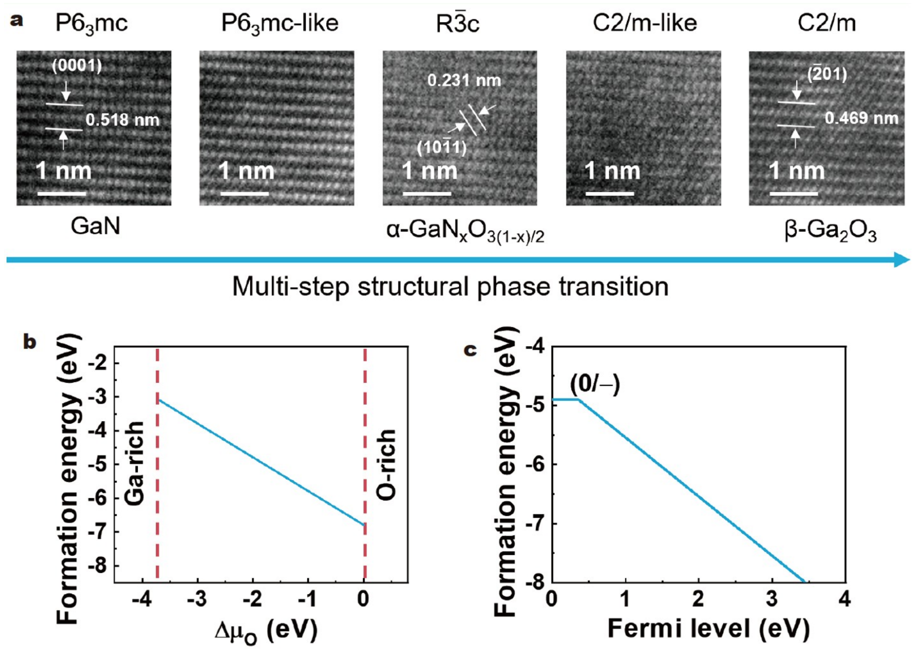

Figure 1 (a) HRTEM images of Sample SP obtained at different locations of the β-Ga_2O_3/GaN interface. (b) Formation energy *versus* chemical potential of O atoms $\Delta\mu_O$. (c) Transition level of the $N_{O(III)}$ acceptor.

devices fabrication.

N-doped β-Ga_2O_3 films with a Ga/O ratio of 0.66 were investigated by XRD, Raman, HRTEM, SAED and XPS (Figs S3 and S4). The positive Hall coefficient indicates the N-doped β-Ga_2O_3 films are p-type (Fig. 2a). XPS and UPS VB analyses further evidence the p-type conductivity of the N-doped β-Ga_2O_3 films. The surface VBM locates at 0.79 eV (0.80 eV) by XPS (UPS) analysis with E_F at 0 eV (Fig. S5). β-Ga_2O_3 usually exihibits a band bending at the surface due to the complex surface states [32,33]. Thus the VB structure extracted from XPS and UPS is usually different from that of the bulk. The Hall hole concentration and mobility of the N-doped β-Ga_2O_3 films are ~1.50×10^{15} cm^{-3} and ~7.99 cm^2 V^{-1} s^{-1}, respectively (Table S1). The average energy difference (ξ_p) between E_F and VBM is calculated to be 0.243 eV from equation: $\xi_p = E_F - E_V = k_BT\ln(N_V/p)$, where E_V is the level of VBM, k_B is the Boltzmann constant, T is the temperature, and N_V is the VB effective density of states. The N_V is calculated to be 1.73×10^{19} cm^{-3} from the equation: $N_V=2\left(\frac{m_p^* k_B T}{2\pi\hbar^2}\right)^{3/2}$, where hole effective mass (m_p^*) of N-doped β-Ga_2O_3 is $0.78m_0$ [34,35]. The acceptor energy level was further estimated by temperature-dependent Hall measurement using the linear regression formula of $\ln(p)$ *versus* $1000/T$. The acceptor ionization energy is ~0.24 eV, which is close to the calculation results (Fig. S6). Typical p-type I–V characteristics are observed for the N-doped β-Ga_2O_3 films FETs with an on/off ratio of 2.4×10^5 at a drain-source voltage (V_{DS}) of 20 V (Fig. 2b), which further evidences the fabrication of the p-type N-doped β-Ga_2O_3 films. The leakage current characteristic of the N-doped β-Ga_2O_3 films FETs indicates a good gate insulation (Fig. S7).

The XRD pattern of the Sn-doped Ga_2O_3/N-doped Ga_2O_3 films shows identified diffraction peaks of β-Ga_2O_3 crystal ($\bar{2}$01), (400), (002), ($\bar{1}$12), ($\bar{4}$02), and ($\bar{6}$03) planes, indicating the formation of pure β-Ga_2O_3 films (Fig. 2c). SIMS elemental mappings of Ga (brown), O (red), Sn (pink), N (blue), and Al (green) over the same film indicate the fabrication of a Sn-doped β-Ga_2O_3/N-doped β-Ga_2O_3 structure (Fig. 2e). Annealing-induced mutual diffusion of low-concentration Sn and N impurities is observed [36,37]. SIMS line profiles (Fig. 2d) indicate that in the top of the Sn-doped β-Ga_2O_3 layer the average Sn and N concentrations are about 2×10^{17} cm^{-3} and 1×10^{16} cm^{-3}, respectively, whereas in the bottom of the N-doped β-Ga_2O_3 layer the average N and Sn concentrations are about 3×10^{18} cm^{-3} and 1×10^{16} cm^{-3}, respectively. A 200-nm interface with a significant decrease of Sn concentration from 2×10^{17} to 2×10^{16} cm^{-3} and an increase of N concentration from 2×10^{16} to 4×10^{17} cm^{-3} (red region, Fig. 2e) is formed between Sn-doped β-Ga_2O_3 and N-doped β-Ga_2O_3.

Sn-doped β-Ga_2O_3 films with a Ga/O ratio of 0.69 were investigated by XPS (Fig. S8). The negative Hall coefficient indicates the Sn-doped β-Ga_2O_3 films are n-type (Fig. 2f). The Hall electron concentration and mobility of the Sn-doped β-Ga_2O_3 films are ~1.69×10^{16} cm^{-3} and ~38.09 cm^2 V^{-1} s^{-1}, respectively (Table S1). The average energy difference (ξ_n) between E_F and conduction band maximum (CBM) is calculated to be 0.148 eV from equation: $\xi_n = E_C - E_F = k_BT\ln(N_C/n)$, where E_C is the level of CBM, and N_C is the CB effective density of states. The N_C is calculated to be 5.02×10^{18} cm^{-3} from equation $N_C=2\left(\frac{m_n^* k_B T}{2\pi\hbar^2}\right)^{3/2}$, where electron effective mass (m_n^*) is $0.342m_0$ according to other calculation results [38,39]. Typical n-type I–V characteristics are observed for the Sn-doped β-Ga_2O_3 films FETs with an on/off ratio of 4.5×10^6 at a V_{DS} of 20 V, which further evidences the fabrication of n-type Sn-doped β-Ga_2O_3 films (Fig. 2g). Thus, the fabrication of full β-Ga_2O_3 films with the n-type Sn-doped β-Ga_2O_3/p-type N-doped β-Ga_2O_3 structure has been demonstrated.

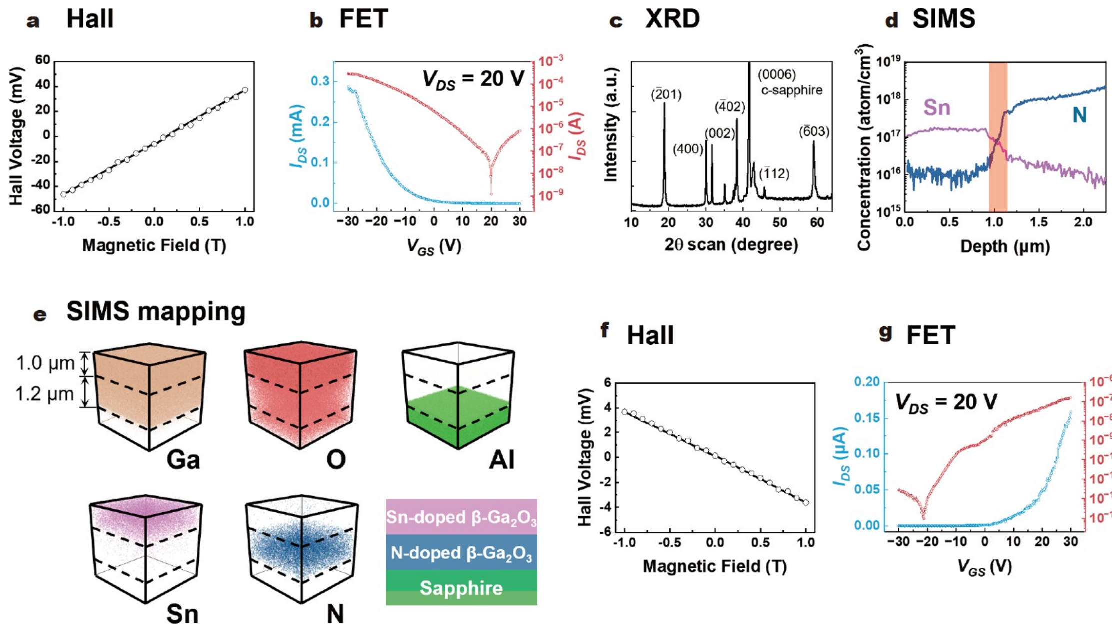

Figure 2 (a) Hall voltage *versus* magnetic field curve from van der Pauw Hall effect measurement of the N-doped β-Ga_2O_3 thin films. (b) Drain-source current (I_{DS}) *versus* gate-source voltage (V_{GS}) characteristic curve of the N-doped β-Ga_2O_3 films top-gate FET in linear and log scale at a drain-source voltage (V_{DS}) of 20 V. (c) XRD spectrum of the Sn-doped β-Ga_2O_3/N-doped β-Ga_2O_3 films on the sapphire substrate. (d) SIMS depth profile of the Sn-doped β-Ga_2O_3/N-doped β-Ga_2O_3 films showing the concentrations of Sn and N. (e) SIMS elemental mappings of Ga (brown), O (red), Al (green), Sn (pink), N (blue) components, and the layer structure of the β-Ga_2O_3 film. (f) Hall voltage *versus* magnetic field curve from van der Pauw Hall effect measurement of the Sn-doped β-Ga_2O_3 thin films. (g) I_{DS} *versus* V_{GS} characteristic curve of the Sn-doped β-Ga_2O_3 back-gate FET in linear and log scale at a V_{DS} of 20 V.

Full β-Ga_2O_3 p-n homojunction diode

Fig. 3a shows a schematic for the β-Ga_2O_3 p-n homojunction diodes with Pad 1/2 on Sn-doped β-Ga_2O_3 and Pad 3/4 on N-doped β-Ga_2O_3. The I–V curve with the applied voltage V_{nn} on Pads 1 and 2 indicates the formation of Ohmic contact between Pad 1/2 and n-type Sn-doped β-Ga_2O_3, and the I–V curve with the applied voltage V_{pp} on Pads 3 and 4 indicates the formation of quasi-Ohmic contact between Pad 3/4 and p-type N-doped β-Ga_2O_3 (Fig. 3b). The $1/C^2$–V curves show that the Schottky barriers are too weak to be detected for both n-type contacts and p-type contacts (Fig. 3c). The forward current *versus* voltage curve of the β-Ga_2O_3 p-n homojunction diodes with the applied voltage V_{pn} on Pads 3 and 1 shows a large forward current density of 4.32 × 10^3 A cm^{-2} at 40 V (Fig. 3d), which is consistent with the simulation results using vertical cross-section area for the current density calculations (Fig. S2). The $R_{on,sp}$ is ~9.18 mΩ cm^2 at 40 V (Fig. 3d), close to that of p-NiO/n-Ga_2O_3 heterojunctions [9,11,12,14,40–42]. The rectification ratio is ~4 × 10^4 at a wide voltage range (Fig. 3e), which is close to the rectification ratios of ZnO p-n junctions, some Ga_2O_3-based p-n heterojunctions, and two-dimensional van-der-Waals p-n junctions [43–50]. The ideal factor η is estimated to be ~1.78 from Shockley diode equation $I = I_s[\exp(V/\eta k_B T) - 1]$. The β-$Ga_2O_3$ p-n homojunction diode was retested after exposure in air for 6 months. The diode shows longterm stability with almost no changes of the I–V characteristics (Fig. 3f). The reverse current of the β-Ga_2O_3 p-n homojunction diode is 5.17 × 10^{-3} A cm^{-2} at −5 V bias and increases to 0.11 A cm^{-2} at −40 V bias, which mainly originates from high-density threading dislocations and the related defects leading to large tunneling current at high reverse bias and can be further suppressed by structure optimization, such as introducing insulating interface layer or field plate structures [41,43,47]. Limited by the semiconductor parameter analyzer we used, the reverse breakdown characteristic is measured from 0 to −200 V. No reverse breakdown characteristic is observed at −200 V, indicating that the breakdown voltage of the β-Ga_2O_3 p-n diode is larger than 200 V (Fig. S9a). The rectifying performance was further explored by applying 100 Hz AC square wave (Fig. 3f) and sine wave (Fig. S9b) from −30 to 30 V on the diode. The time-dependent input voltage and rectified output current characteristics of the β-Ga_2O_3 p-n diode show good rectification behavior without overshoot during voltage on. The rectification ratio is ~6.60 × 10^4 under the low frequency AC voltage, and the rise and decay time are 50 and 10 μs, respectively.

Band structure analysis of the β-Ga_2O_3 p-n homojunction diode

Fig. 4a shows the junction capacitance (C_p) *versus* applied voltage curve of the β-Ga_2O_3 p-n diode. The depletion capacitance dominates at the region of $V < V_{bi}$ and diffusion capacitance dominates at the region of $V > V_{bi}$. Depletion capacitance is in parallel with diode resistance and diffusion capacitance is in series with diode resistance. C–V characteristic contains junction characteristics of β-Ga_2O_3 p-n diode, such as V_{bi}, depletion width and carrier concentration. C_p grows from 1 nF cm^{-2} at reverse bias to 4 nF cm^{-2} at V_{bi}, which is a small capacitance variation due to the thin film thickness and depletion layer. Low depletion capacitance improves the speed of switching device.

The V_{bi} in the β-Ga_2O_3 p-n diode is estimated to be 4.41 V from the $1/C_p^2$–V plot (Fig. 4b), based on junction C–V equation: $C = \sqrt{\frac{q\varepsilon N_a N_d}{2(N_a + N_d)}}(V_{bi} - V)^{-\frac{1}{2}}$, where ε is the dielectric constant, N_a is the free hole concentration, N_d is the free electron concentration, and q is the charge of an electron. By extracting

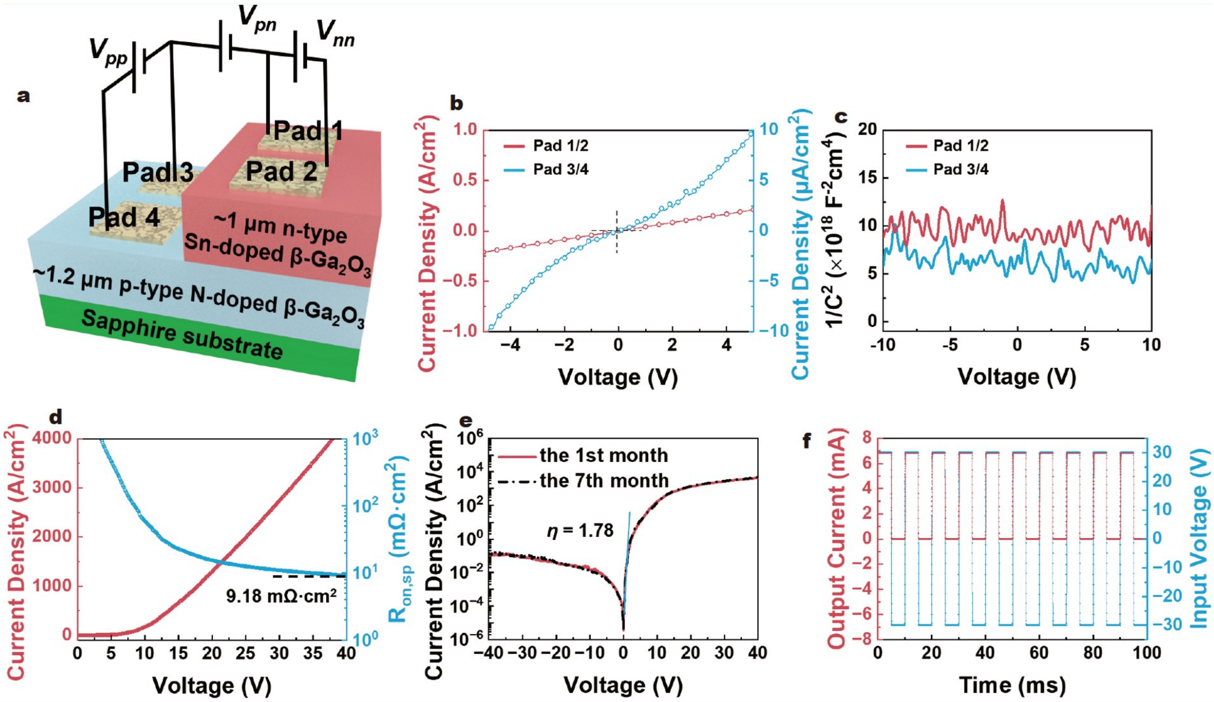

Figure 3 (a) Schematic of the n-type Sn-doped β-Ga_2O_3/p-type N-doped β-Ga_2O_3 homojunction diode (V_{pn}). (b) *I*–*V* and (c) *C*–*V* curves with the applied voltage V_{nn} on Pad 1/2 and the applied voltage V_{pp} on Pad 3/4. (d) Forward current density and $R_{on,sp}$ *versus* applied voltage curve. (e) Current density *versus* voltage curves of the β-Ga_2O_3 p-n homojunction diode measured on the first month and the seventh month. (f) Rectified output current using the β-Ga_2O_3 diode by applying an AC square wave.

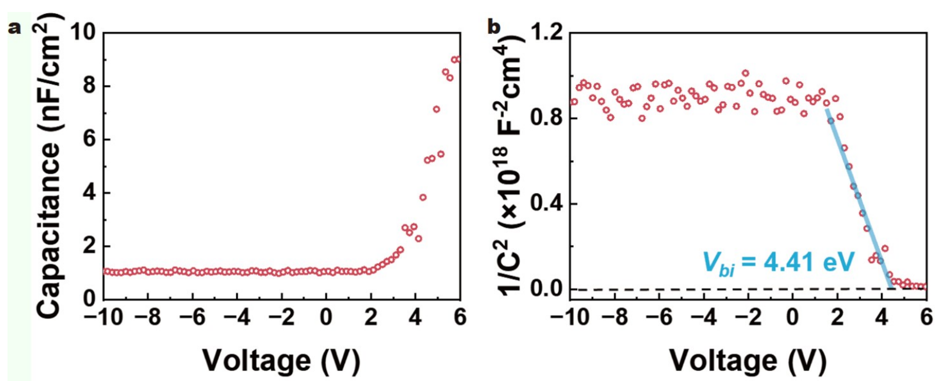

Figure 4 (a) C_p–V and (b) $1/C_p^2$–V characteristics of the β-Ga_2O_3 p-n homojunction diode.

the slope of $1/C_p^2$–V, the hole and electron concentrations are estimated to be ~1.14×10^{15} and ~1.14×10^{16} cm^{-3}, respectively, in agreement with the Hall measurements. A depletion width is calculated to be 0.8 μm in the β-Ga_2O_3 p-n diode. The p-type and n-type depletion widths (W_p and W_n) are calculated to be 734.8 and 65.2 nm, respectively, derived from equations $W=\sqrt{\frac{2\varepsilon V_{bi}(N_a+N_d)}{qN_aN_d}}$ and $N_aW_p=N_dW_n$, where W is the width of depletion region, N_a is the Hall hole concentration of ~1.50×10^{15} cm^{-3}, and N_d is the Hall electron concentration of ~1.69×10^{16} cm^{-3}. p-type N-doped β-Ga_2O_3 layer contributes more to the depletion region than n-type Sn-doped layer β-Ga_2O_3 because of the low hole concentration.

Fig. 5a shows the schematic energy band diagrams for the isolated p-type N-doped β-Ga_2O_3 and n-type Sn-doped β-Ga_2O_3. The electron concentration is much larger than the hole concentration (Table S1) and thus the simulated band diagram (Fig. S10) shows an abrupt change at the n-type region, which preliminarily confirms that the β-Ga_2O_3 p-n homojunction is a one-sided abrupt p-n junction. Fig. 5b shows the energy band diagram for the β-Ga_2O_3 p-n homojunction. The electron affinity and the bandgap of β-Ga_2O_3 are typically 4.00 and 4.85 eV, respectively [51,52]. The average E_{Fp} and E_{Fn} of the p-type N-doped β-Ga_2O_3 and n-type Sn-doped β-Ga_2O_3 locate at 0.243 and 4.702 eV with VBM at 0 eV, respectively. The V_{bi} is 4.459 V as estimated from ξ_p and ξ_n, which is close to the *C*–*V* measured V_{bi} of 4.41 V. Fig. 5c shows the simplified energy band diagrams and carrier characteristic under bias conditions. Under low forward bias ($0 < V < V_{bi}$), the electric field within the p-n junction, depletion layer width, and the potential barrier (V_{bi} –

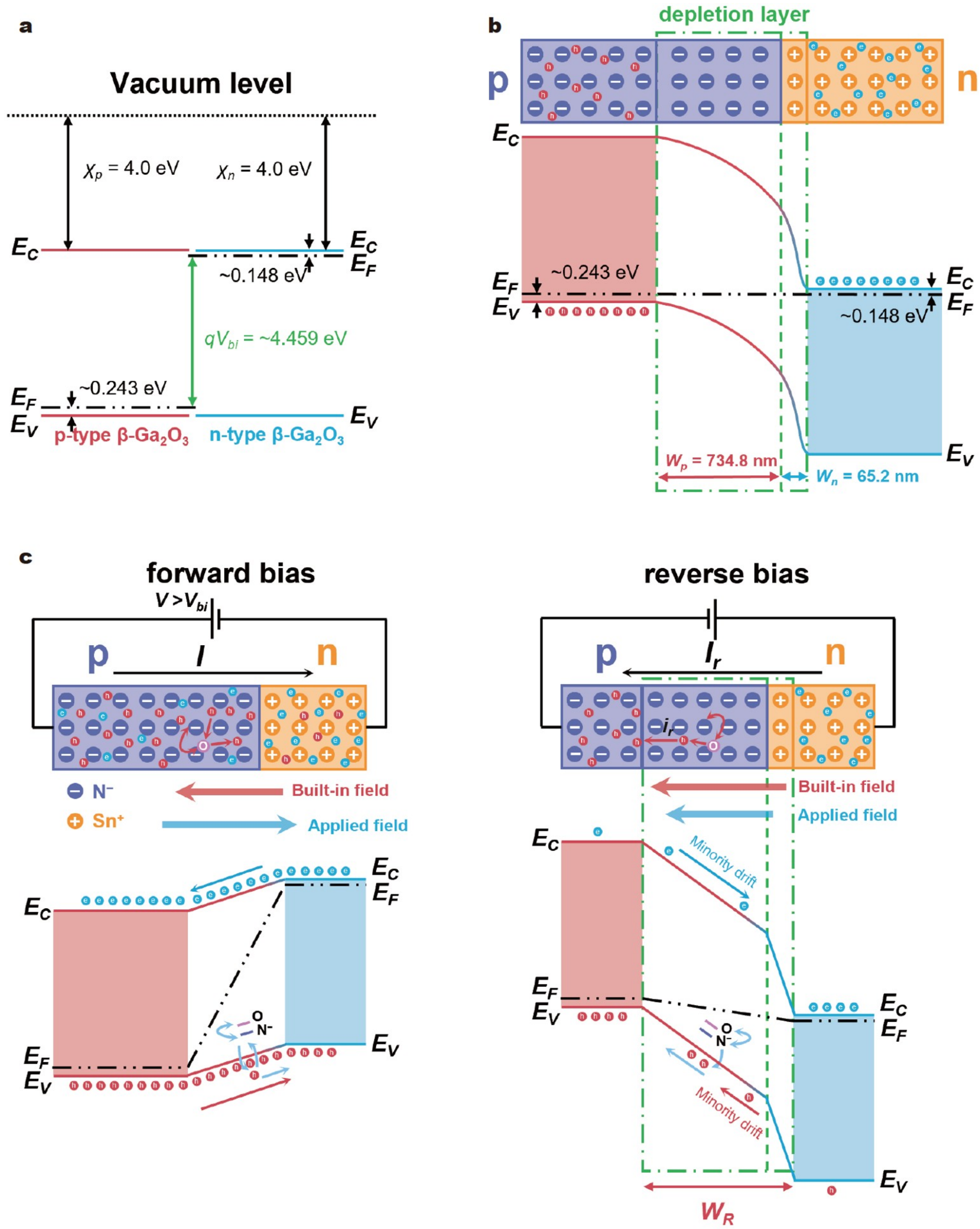

Figure 5 Schematic band diagrams of (a) p-type and n-type β-Ga_2O_3, and (b) β-Ga_2O_3 p-n homojunction. (c) Schematic band diagrams and internal mechanisms of β-Ga_2O_3 p-n homojunction under different biases.

V) for the majority carriers across the junction decreases with the increase of the applied voltage V. Under high forward bias ($V > V_{bi}$), a small increase in the applied voltage results in a significant increase of current flow across the junction (Fig. 3d). The charge carrier injection may also lead to trapping/de-trapping of holes and excitons, which is enhanced by the N acceptor impurities induced VB engineering and delocalization effect (Fig. S11), and charge carrier recombination within the p-n junction diode. The ideal factor η of ~1.78 (Fig. 3e) indicates the presence of charge carrier recombination current as well as diffusion current. Under reverse bias the electric field within the p-n junction, depletion layer width, and the potential barrier (V_{bi} + V) increases with the increase of reverse bias voltage V. As a result, the reverse current I_r is very low mainly contributed by the thermionic minority carrier injection [10]. Further increase of the reverse bias and electric field within the p-n junction may result in the de-trapping/trapping of holes and excitons, generating an additional reverse current i_r. The high reverse leakage current at high reverse bias is attributed to minority carrier drift, de-trapping/trapping of holes and excitons, thermionic emission, Shockley–Read–Hall recombination and Variable–Range Hopping [53] which originate from impurities, defects and dislocations.

CONCLUSIONS

N-doped β-Ga_2O_3 films is constructed by a from-GaN-to-β-Ga_2O_3 structural phase transition technique, which is followed by sputter deposition of Sn-doped β-Ga_2O_3 thin film on the N-doped β-Ga_2O_3 films. The n-type Sn-doped β-Ga_2O_3/p-type N-doped β-Ga_2O_3 thin films are demonstrated by the TEM, XRD, DFT calculations, Hall, and FET I–V analyses. The Hall electron concentration and hole concentration are 1.69×10^{16} and 1.50×10^{15} cm^{-3}, respectively. The full β-Ga_2O_3 thin film one-sided abrupt p-n homojunction diodes fabricated on the Sn-doped β-Ga_2O_3/N-doped β-Ga_2O_3 films show a high rectification ratio of 4×10^4, a low $R_{on,sp}$ of 9.18 mΩ cm^2, and a high forward current density of 4.32×10^3 A cm^{-2} at 40 V, a V_{bi} of 4.41 V, a junction depletion width of 0.8 μm, an ideal factor of 1.78, good rectification behavior under AC voltage without overshoot, and longtime stability. The first demonstration of full β-Ga_2O_3 thin film one-sided abrupt p-n homojunction diodes lays the foundation for β-Ga_2O_3 homogeneous bipolar devices and paves the way for the evolution of high-voltage and high-power device applications.

Received 9 October 2023; accepted 26 December 2023; published online 23 January 2024

1 Peelaers H, Lyons JL, Varley JB, *et al.* Deep acceptors and their diffusion in Ga_2O_3. APL Mater, 2019, 7: 022519
2 Stampfl C, Van de Walle CG. Doping of $Al_xGa_{1-x}N$. Appl Phys Lett, 1998, 72: 459–461
3 Lu S, Shen P, Zhang H, *et al.* Towards n-type conductivity in hexagonal boron nitride. Nat Commun, 2022, 13: 3109
4 Sharma R, Law ME, Ren F, *et al.* Diffusion of dopants and impurities in β-Ga_2O_3. J Vacuum Sci Tech A-Vacuum Surfs Films, 2021, 39: 060801
5 Chikoidze E, Fellous A, Perez-Tomas A, *et al.* p-type β-gallium oxide: A new perspective for power and optoelectronic devices. Mater Today Phys, 2017, 3: 118–126
6 Lyons JL. A survey of acceptor dopants for β-Ga_2O_3. Semicond Sci Technol, 2018, 33: 05LT02
7 Neal AT, Mou S, Rafique S, *et al.* Donors and deep acceptors in β-Ga_2O_3. Appl Phys Lett, 2018, 113: 062101
8 Islam MM, Rana D, Hernandez A, *et al.* Study of trap levels in β-Ga_2O_3 by thermoluminescence spectroscopy. J Appl Phys, 2019, 125: 055701
9 Lu X, Zhou X, Jiang H, *et al.* 1-kV sputtered p-NiO/n-Ga_2O_3 heterojunction diodes with an ultra-low leakage current below μA/cm^2. IEEE Electron Device Lett, 2020, 41: 449–452
10 Gong H, Chen X, Xu Y, *et al.* Band alignment and interface recombination in NiO/β-Ga_2O_3 type-II p-n heterojunctions. IEEE Trans Electron Devices, 2020, 67: 3341–3347
11 Gong HH, Chen XH, Xu Y, *et al.* A 1.86-kV double-layered NiO/β-Ga_2O_3 vertical p-n heterojunction diode. Appl Phys Lett, 2020, 117: 022104
12 Hao W, He Q, Zhou K, *et al.* Low defect density and small I–V curve hysteresis in NiO/β-Ga_2O_3 pn diode with a high PFOM of 0.65 GW/cm^2. Appl Phys Lett, 2021, 118: 043501
13 Liu Y, Wang L, Zhang Y, *et al.* Demonstration of n-Ga_2O_3/p-GaN diodes by wet-etching lift-off and transfer-print technique. IEEE Electron Device Lett, 2021, 42: 509–512
14 Wang C, Gong H, Lei W, *et al.* Demonstration of the p-NiO_x/n-Ga_2O_3 heterojunction gate FETs and diodes with BV^2/$R_{on,sp}$ figures of merit of 0.39 GW/cm^2 and 1.38 GW/cm^2. IEEE Electron Device Lett, 2021, 42: 485–488
15 Wang H, Xiang G, Zhou Y, *et al.* Excellent electroluminescence and electrical characteristics from p-CuO/i-Ga_2O_3/n-GaN light-emitting diode prepared by magnetron sputtering. J Lumin, 2022, 243: 118621
16 Zhang ZH, Liu W, Ju Z, *et al.* Self-screening of the quantum confined Stark effect by the polarization induced bulk charges in the quantum barriers. Appl Phys Lett, 2014, 104: 243501
17 Zhang ZH, Liu W, Ju Z, *et al.* InGaN/GaN multiple-quantum-well light-emitting diodes with a grading InN composition suppressing the Auger recombination. Appl Phys Lett, 2014, 105: 33506
18 Clinton EA, Engel Z, Vadiee E, *et al.* Ultra-wide-bandgap AlGaN homojunction tunnel diodes with negative differential resistance. Appl Phys Lett, 2019, 115: 082104
19 Dhruv SD, Dhruv DK. Anomalous current–voltage and impedance behaviour in heterojunction diode. Mater Today-Proc, 2022, 55: A1–A6
20 Chikoidze E, Sartel C, Mohamed H, *et al.* Enhancing the intrinsic p-type conductivity of the ultra-wide bandgap Ga_2O_3 semiconductor. J Mater Chem C, 2019, 7: 10231–10239
21 Cai X, Sabino FP, Janotti A, *et al.* Approach to achieving a p-type transparent conducting oxide: Doping of bismuth-alloyed Ga_2O_3 with a strongly correlated band edge state. Phys Rev B, 2021, 103: 115205
22 Su Y, Guo D, Ye J, *et al.* Deep level acceptors of Zn-Mg divalent ions dopants in β-Ga_2O_3 for the difficulty to p-type conductivity. J Alloys Compd, 2019, 782: 299–303
23 Zhang C, Li Z, Wang W. Critical thermodynamic conditions for the formation of p-type β-Ga_2O_3 with Cu doping. Materials, 2021, 14: 5161
24 Wang D, Ge K, Meng D, *et al.* p-type β-Ga_2O_3 films were prepared by Zn-doping using RF magnetron sputtering. Mater Lett, 2023, 330: 133251
25 Zhou X, Li M, Zhang J, *et al.* High quality p-type Mg-doped β-$Ga_2O_{3-\delta}$ films for solar-blind photodetectors. IEEE Electron Device Lett, 2022, 43: 580–583
26 Ebrahimi-Darkhaneh H, Shekarnoush M, Arellano-Jimenez J, *et al.* High-quality Mg-doped p-type Ga_2O_3 crystalline thin film by pulsed laser. J Mater Sci-Mater Electron, 2022, 33: 24244–24259
27 Chikoidze E, Sartel C, Yamano H, *et al.* Electrical properties of p-type Zn:Ga_2O_3 thin films. J Vacuum Sci Tech A, 2022, 40: 043401
28 Saikumar AK, Sundaresh S, Sundaram KB. Preparation and characterization of p-type copper gallium oxide ($CuGaO_2$) thin films by dual sputtering using Cu and Ga_2O_3 targets. ECS J Solid State Sci Technol, 2022, 11: 065010
29 Bai R, Zhao B, Ling K, *et al.* Dilute-selenium alloying: A possible perspective for achieving p-type conductivity of β-gallium oxide. J Alloys Compd, 2022, 891: 161969
30 Wu ZY, Jiang ZX, Ma CC, *et al.* Energy-driven multi-step structural phase transition mechanism to achieve high-quality p-type nitrogen-doped β-Ga_2O_3 films. Mater Today Phys, 2021, 17: 100356
31 Jiang ZX, Wu ZY, Ma CC, *et al.* p-type β-Ga_2O_3 metal-semiconductor-metal solar-blind photodetectors with extremely high responsivity and gain-bandwidth product. Mater Today Phys, 2020, 14: 100226
32 Lovejoy TC, Chen R, Zheng X, *et al.* Band bending and surface defects in β-Ga_2O_3. Appl Phys Lett, 2012, 100: 181602
33 Navarro-Quezada A, Alamé S, Esser N, *et al.* Near valence-band electronic properties of semiconducting β-Ga_2O_3 (100) single crystals. Phys Rev B, 2015, 92: 1–5
34 Ma C, Wu Z, Jiang Z, *et al.* Exploring the feasibility and conduction mechanisms of p-type nitrogen-doped β-Ga_2O_3 with high hole mobility. J Mater Chem C, 2022, 10: 6673–6681
35 Ma C, Wu Z, Zhang H, *et al.* p-type nitrogen-doped β-Ga_2O_3: The role of stable shallow acceptor N_O-V_{Ga} complexes. Phys Chem Chem Phys, 2023, 25: 13766–13771
36 Kuroda N, Sasaoka C, Kimura A, *et al.* Precise control of pn-junction profiles for GaN-based LD structures using GaN substrates with low dislocation densities. J Cryst Growth, 1998, 189-190: 551–555
37 Yoshizumi Y, Hashimoto S, Tanabe T, *et al.* High-breakdown-voltage pn-junction diodes on GaN substrates. J Cryst Growth, 2007, 298: 875–878
38 He H, Orlando R, Blanco MA, *et al.* First-principles study of the structural, electronic, and optical properties of Ga_2O_3 in its monoclinic and hexagonal phases. Phys Rev B, 2006, 74: 195123
39 Fan Q, Zhao R, Zhang W, *et al.* Low-energy Ga_2O_3 polymorphs with low electron effective masses. Phys Chem Chem Phys, 2022, 24: 7045–7049
40 Zhang J, Dong P, Dang K, *et al.* Ultra-wide bandgap semiconductor Ga_2O_3 power diodes. Nat Commun, 2022, 13: 3900
41 Gong H, Yu X, Xu Y *et al.* Vertical field-plated NiO/Ga_2O_3 heterojunction power diodes. In: 2021 5th IEEE Electron Devices Technology & Manufacturing Conference (EDTM). Chengdu: IEEE, 2021. 1–3
42 Shimbori A, Wong HY, Huang AQ. Fabrication and analysis of a novel high voltage heterojunction p-NiO/n-Ga_2O_3 diode. In: 2020 32nd International Symposium on Power Semiconductor Devices and ICs (ISPSD). Vienna: IEEE, 2020. 218–221
43 Snigurenko D, Guziewicz E, Krajewski TA, *et al.* N and Al co-doping as

a way to p-type ZnO without post-growth annealing. Mater Res Express, 2016, 3: 125907
44 Kumari C, Pandey A, Dixit A. Improved rectification behaviour in ZnO nanorods homojunction by suppressing Li donor defects using Li-Ni co-doping. Superlattices MicroStruct, 2019, 132: 106154
45 Wu G, Tian B, Liu L, *et al.* Programmable transition metal dichalcogenide homojunctions controlled by nonvolatile ferroelectric domains. Nat Electron, 2020, 3: 43–50
46 Zhong F, Ye J, He T, *et al.* Substitutionally doped $MoSe_2$ for high-performance electronics and optoelectronics. Small, 2021, 17: 2102855
47 A SM, Joseph JA, Nair BG, *et al.* Enhanced photocatalytic activity of nZnO/n^+ Al:ZnO homojunction with an overlayer of Al_2O_3 nanoballs. J Phys D-Appl Phys, 2022, 55: 175108
48 Li Y, Xiao J, Cao X, *et al.* Lateral WSe_2 homojunction through metal contact doping: Excellent self-powered photovoltaic photodetector. Adv Funct Mater, 2023, 33: 2213385
49 Tan C, Wang H, Zhu X, *et al.* A self-powered photovoltaic photodetector based on a lateral WSe_2-WSe_2 homojunction. ACS Appl Mater Interfaces, 2020, 12: 44934–44942
50 Li Q, Du BD, Gao JY, *et al.* Liquid metal gallium-based printing of Cu-doped p-type Ga_2O_3 semiconductor and Ga_2O_3 homojunction diodes. Appl Phys Rev, 2023, 10: 011402
51 Mohamed M, Irmscher K, Janowitz C, *et al.* Schottky barrier height of Au on the transparent semiconducting oxide β-Ga_2O_3. Appl Phys Lett, 2012, 101: 132106
52 Janowitz C, Scherer V, Mohamed M, *et al.* Experimental electronic structure of In_2O_3 and Ga_2O_3. New J Phys, 2011, 13: 085014
53 Shklovskii BI, Efros AL. Variable-range hopping conduction. In: Shklovskii BI, Efros AL. Electronic Properties of Doped Semiconductors. Berlin, Heidelberg: Springer, 1984. 202–227

Acknowledgements This work was supported by the National Key R&D Program of China (2022YFB3605500 and 2022YFB3605503), the National Natural Science Foundation of China (62074039 and 12004074), China Postdoctoral Science Foundation (2020M681141), and the National Postdoctoral Program for Innovative Talents (BX20190070).

Author contributions Fang Z conceived the idea. Fang Z, Zhai H and Wu Z designed the experiments. Zhai H and Liu C carried out the material synthesis and characterized the β-Ga_2O_3 p-n homojunction. Ma C, Zhai H, Fang Z and Wu Z contributed to the theoretical calculations. Zhai H and Fang Z drafted the manuscript. Fang Z, Zhai H, Liu C, Wu Z, Ma C, Tian P, Wan J, Kang J and Chu J revised and proofread the manuscript.

Conflict of interest The authors declare that they have no conflict of interest.

Supplementary information Supporting data are available in the online version of the paper.

Hongchao Zhai received his Bachelor's degree in electrical engineering and automation from Fudan University and now is pursuing his PhD degree in physical electronics at Fudan University. His current research focuses on the β-Ga_2O_3 devices, including p-n junctions and gas sensors.

Zhilai Fang received his PhD degree from the Chinese University of Hong Kong and worked as a postdoctoral researcher at Humboldt University of Berlin. He is currently a professor at the School of Information Science and Technology, Fudan University. His current research focuses on the β-Ga_2O_3-based materials and devices.

全氧化镓薄膜同质p-n结

翟泓超[1], 刘晨星[1], 吴征远[1,2], 马聪聪[1], 田朋飞[1], 万景[1], 康俊勇[3], 褚君浩[2], 方志来[1,2*]

摘要 制备p-n结以及探索其物理机制在发展各种功能器件和推进其实际应用中起到关键作用. 超宽禁带半导体在制备高压高频器件上有着巨大的潜力，但是氧化镓p型掺杂困难限制了氧化镓同质p-n结的制备，进而阻碍了全氧化镓基双极型器件的发展. 本文通过一种先进的相转变生长技术结合溅射镀膜的方法，成功制备了n型锡掺杂β相氧化镓/p型氮掺杂β相氧化镓薄膜. 本工作成功制作了全氧化镓单边突变同质p-n结二极管，并且详细分析了器件机理. 该二极管实现了4 × 10^4的整流比、在40 V下9.18 mΩ cm^2的低导通电阻、4.41 V的内建电势和1.78的理想因子，并在交流电压下表现出没有过冲的整流特性以及长期稳定性. 本工作为氧化镓同质p-n结初窥门径，为氧化镓同质双极型器件奠定了基础，为高压高功率器件的应用开创了道路.